Hindawi Publishing Corporation
EURASIP Journal on Wireless Communications and Networking
Volume 2010, Article ID 721695, 10 pages
doi:10.1155/2010/721695

Research Article

Higher-Order Cyclostationarity Detection for Spectrum Sensing

Julien Renard, Jonathan Verlant-Chenet, Jean-Michel Dricot, Philippe De Doncker, and Francois Horlin

Université Libre de Bruxelles, Avenue F. D. Roosevelt 50, 1050 Brussels, Belgium

Correspondence should be addressed to Julien Renard, jrenard.ulb@gmail.com

Received 30 September 2009; Revised 18 February 2010; Accepted 15 June 2010

Academic Editor: André Bourdoux

Recent years have shown a growing interest in the concept of Cognitive Radios (CRs), able to access portions of the electromagnetic spectrum in an opportunistic operating way. Such systems require efficient detectors able to work in low Signal-to-Noise Ratio (SNR) environments, with little or no information about the signals they are trying to detect. Energy detectors are widely used to perform such blind detection tasks, but quickly reach the so-called SNR wall below which detection becomes impossible Tandra (2005). Cyclostationarity detectors are an interesting alternative to energy detectors, as they exploit hidden periodicities present in man-made signals, but absent in noise. Such detectors use quadratic transformations of the signals to extract the hidden sine-waves. While most of the literature focuses on the second-order transformations of the signals, we investigate the potential of higher-order transformations of the signals. Using the theory of Higher-Order Cyclostationarity (HOCS), we derive a fourth-order detector that performs similarly to the second-order ones to detect linearly modulated signals, at SNR around 0 dB, which may be used if the signals of interest do not exhibit second-order cyclostationarity. More generally this paper reviews the relevant aspects of the cyclostationary and HOCS theory, and shows their potential for spectrum sensing.

1. Introduction

Many studies have shown that the static frequency allocation for wireless communication systems is responsible for the inefficient use of the spectrum [1]. This is so because the systems are not continuously transmitting. Cognitive Radios (CRs) networks try to make use of the gaps that can be found in the spectrum at a given time. This opportunistic behavior categorizes CR as secondary users of a given frequency band, by contrast with the systems that were permanently assigned this band (primary users) [2]. For the CR concept to be viable, it is required that it does not interfere with the primary user services. It means that the system must be able to detect primary user signals in low signal-to-noise ratio (SNR) environments fast enough. Efforts are being made to improve the performance of the detectors [3].

A radiometer (also called energy detector) can be used to detect completely unknown signals in a determined frequency band [4]. It is historically the oldest and simplest detector, and it achieves good performance when the SNR is strong enough. Unfortunately, since it is based on an estimation of the in-band noise power spectral density (PSD), it is affected by the noise level uncertainty (due to measurement errors or a changing environment), especially at low SNR [5], where it reaches an absolute performance limit called the SNR wall. Another type of detector is based on the spectral redundancy present in almost every man-made signal. It is called a cyclic feature detector and will be the kind of detector of interest in this paper.

Cyclic feature detectors make use of the cyclostationarity theory, which can be divided in two categories: the second-order cyclostationarity (SOCS) introduced by Gardner in [6–8] and the higher-order cyclostationarity (HOCS) introduced by Gardner and Spooner in [9, 10]. The SOCS uses quadratic nonlinearities to extract sine-waves from a signal, whereas the HOCS is based on nth-order nonlinearities. The idea behind this theory is that man-made signals possess hidden periodicities such as the carrier frequency, the symbol rate or the chip rate, that can be regenerated by a sine-wave extraction operation which produces features at frequencies that depend on these hidden periodicities (hence called cyclic features and cycle frequencies resp.). Since the SOCS is based on quadratic nonlinearities, two frequency parameters are used for the sine-wave extraction function. The result is

called the spectral correlation density (SCD), and can be represented in a bifrequency plane. The SCD can be seen as a generalization of the PSD, as it is equal to the PSD when the cycle frequency is equal to zero. Therefore, the SOCS cyclic feature detectors act like energy detectors, but at cycle frequencies different from zero. The advantage of these detectors comes from the absence of features (at least asymptotically) when the input signal is stationary (such as white noise), since no hidden frequencies are present, or when the input signal exhibits cyclostationarity at cycle frequencies different than the one of interest. The HOCS cyclic-feature detectors are based on the same principles, but the equivalent of the SCD is a n-dimensional space ($n > 2$). Like SOCS detectors, HOCS detectors have originally been introduced in the literature to blindly estimate the signal frequency parameters.

It has been shown that the second-order cyclostationarity detectors perform better than the energy detectors in low SNR environments [7], and this has recently triggered a lot of research on the use of cyclostationarity detectors for spectrum sensing in the context of cognitive radios [11, 12]. However the second-order detectors suffer from a higher computational complexity that has just become manageable. First field-programmable gate array (FPGA) implementations are presented in [13, 14].

Higher-order detectors are generally even more complex, and since the variance of the features estimators increases when the order rises, most research results concern second-order detectors. We will nevertheless demonstrate that it is possible to derive fourth-order detectors that bear comparable performances to second-order ones to detect linearly modulated baseband signals at SNR around 0 dB. The paper will include a mathematical analysis of the detection algorithm, the effects of each of its parameters and its computational complexity. Performance will be assessed through simulations and compared with the second-order detector.

After introducing the system model in Section 2, we will briefly review the basic notions of cyclostationarity theory in Section 3 in order to understand how second-order detectors work and identify their limitations. Afterwards, we will move on to HOCS theory, and present its most relevant aspects in Section 4, which will be used to characterize the linearly modulated signals in Section 5 and to derive an algorithm that may be used for signal detection of linearly modulated signals in Section 6. We will conclude by a comparison of the new detector performance with second-order detector and energy detector performances in Section 7.

2. System Model

This paper focuses on the detection of linearly modulated signals, like pulse amplitude modulation (PAM) or quadrature amplitude modulation (QAM) signals. The baseband transmitted signal is usually expressed as

$$s(t) = \sum_{m=-\infty}^{\infty} I_m \; p(t - mT_s), \tag{1}$$

where I_m is the sequence of information symbols transmitted at the rate $F_s = 1/T_s$ and $p(t)$ is the pulse shaping filter (typically a square-root Nyquist filter). After baseband-to-radio frequency (RF) conversion, the RF transmitted signal is given by:

$$s^{\mathrm{RF}}(t) = \Re[s(t)]\cos(\omega_c t) - \Im[s(t)]\sin(\omega_c t), \tag{2}$$

where $\omega_c = 2\pi f_c$ and f_c is the carrier frequency. In the PAM case, the symbols I_m are real and only the cosine is modulated. In the QAM case, the symbols I_m are complex and both the cosine and sine are modulated. A QAM signal can be seen as two uncorrelated PAM signals modulated in quadrature.

For the sake of clarity, we assume that the signal propagates through an ideal channel. Our results can nevertheless be extended to the case of multipath channels, if we consider a new pulse shape that is equal to the convolution of square-root Nyquist filter with the channel impulse response. However, this would make the new pulse random. Simulations have shown that both second-order and fourth-order detectors are affected in the same way by a multipath channel (equivalent degradation of performances). Therefore it does not seem critical to introduce multipath channels in order to compare the two, and it allows us to work with a constant pulse shape. Additive white Gaussian noise (AWGN) of one-sided PSD equal to N_0 corrupts the signal at the receiver. Some amount of noise uncertainty can be added to N_0. The detection of the signal at the receiver can be either done directly in the RF domain or in the baseband domain after RF-to-baseband conversion.

3. Second-Order Cyclostationarity

Two approaches are used to introduce the notion of cyclostationarity [8]. While the first approach introduces the temporal features of cyclostationary signals, the second approach is more intuitive and is based on a graphical representation of spectral redundancy. Both approaches lead to the same conclusion. This section reviews the main results of the second-order cyclostationarity theory, which will be generalized to higher-order cyclostationarity in the next sections.

3.1. Temporal Redundancy. A wide-sense cyclostationary signal $x(t)$ exhibits a periodic autocorrelation function [6, 7]

$$R_x(t,\tau) := \mathrm{E}[x(t)x^*(t-\tau)], \tag{3}$$

where $\mathrm{E}[\cdot]$ denotes the statistical expectation operator. Since $R_x(t,\tau)$ is periodic, it can be decomposed in a Fourier series

$$R_x(t,\tau) = \sum_{\alpha} R_x^{\alpha}(\tau) e^{j2\pi\alpha t}, \tag{4}$$

where the sum is over integer multiples of the fundamental frequencies. The coefficient $R_x^{\alpha}(\tau)$ is called the cyclic autocorrelation function, and represents the Fourier coefficient of the series given by

$$R_x^{\alpha}(\tau) = \frac{1}{T_0}\int_{t=-T_0/2}^{T_0/2} R_x(t,\tau)\; e^{-j2\pi\alpha t} dt. \tag{5}$$

When the signal is cyclo-ergodic, the expectation in the definition of the autocorrelation can be replaced by a time average so that

$$R_x^\alpha(\tau) = \lim_{T\to\infty} \frac{1}{T} \int_{t=-T/2}^{T/2} x(t)\, x^*(t-\tau)\, e^{-j2\pi\alpha t} dt\,. \quad (6)$$

The cyclic autocorrelation is therefore intuitively obtained by extracting the frequency α sine-wave from the time-delay product $x(t)\, x^*(t-\tau)$. The SCD $S_x^\alpha(f)$ is defined as the Fourier transform of $R_x^\alpha(\tau)$ over τ. We notice that the only cyclic frequencies α for which the SCD will not be null are the ones corresponding to the Fourier coefficients.

3.2. Spectral Redundancy. Let $X(f)$ be the Fourier transform of $x(t)$. The SCD measures the degree of spectral redundancy between the frequencies $f - \alpha/2$ and $f + \alpha/2$ (α being called the cyclic frequency). It can be mathematically expressed as the correlation between two frequency bins centered on $f - \alpha/2$ and $f + \alpha/2$ when their width tends toward zero [6, 7]

$$S_x^\alpha(f) = \lim_{T\to\infty} \lim_{\Delta t\to\infty} \frac{1}{T\Delta t} \int_{t=-\Delta t/2}^{\Delta t/2} X_T\left(t, \frac{f+\alpha}{2}\right) X_T^*\left(t, \frac{f-\alpha}{2}\right) dt, \quad (7)$$

where $X_T(t, f)$ denotes the short-time Fourier transform of the signal

$$X_T(t, f) = \int_{u=t-T/2}^{t+T/2} x(u)\, e^{-j2\pi f u} du\,. \quad (8)$$

Since the SCD depends on f and α, it can be graphed as a surface over the bifrequency plane (f, α). When $\alpha = 0$, the SCD reduces to the PSD.

3.3. Baseband and RF Second-Order Features. The performance of the cyclic feature detectors will first depend on the strength of the features they are trying to estimate. The two most common features exploited to detect the linearly modulated signals are linked with the symbol rate and the carrier frequency.

(i) The symbol rate feature is usually exploited after RF-to-baseband conversion at the receiver. As its name suggests it, it originates from the symbol rate at the transmitter. Since this is a discrete signal, its frequency spectrum is periodic, with a period equal to the inverse of the sample rate (which is equal to the symbol rate before RF conversion). If there is some excess bandwidth in the system, or in other words, if the pulse shaping filter $p(t)$ does not totally cut off the frequency components larger than half the inverse of the symbol rate, some frequencies will be correlated, as shown in Figure 1.

(ii) The doubled-carrier frequency feature is directly exploited in the RF domain. It is based on the symmetry of the RF spectrum, and it is much stronger than the symbol rate feature (it is as strong as the PSD). Since it depends on the symmetry of the spectrum of the baseband signal, it only exists if the modulation used has no quadrature components. If a real PAM scheme is used, the carrier feature exists, as illustrated in the left part of Figure 2. If a complex QAM scheme is used, the carrier feature vanishes, as illustrated in the right part of Figure 2.

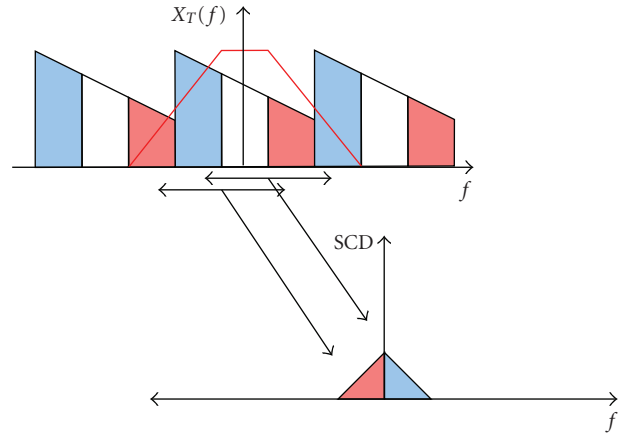

Figure 1: Baseband signal frequency spectrum (top) and SCD at the symbol rate (bottom). The frequency spectrum results from the repetitive discrete signal spectrum and the filter shaping. The SCD is measured by the correlation between two frequency bins centered on $f - \alpha/2$ and $f + \alpha/2$ where α is the symbol rate. The symbol rate feature exists for baseband PAM/QAM signals if there is some excess bandwidth in the system.

Since complex modulations are quite common, it would not be possible to implement a cyclic feature detector for CRs based on the doubled-carrier frequency feature. On the other hand, the symbol rate feature solely depends on the pulse shaping filter. Provided that there is some excess bandwidth, the symbol rate feature will exist, whatever the modulation. Unfortunately, that feature is relatively small and depends on the amount of excess bandwidth. We can therefore ask ourselves if it would not be possible to find greater features using a fourth-order detector.

4. Higher-Order Cyclostationarity

The higher-order cyclostationarity (HOCS) theory is a generalization of the second-order cyclostationarity theory, which only deals with second-order moments, to nth-order moments [9, 10]. It makes use of the fraction-of-time (FOT) probability framework (based on time averages of the signals) which is closely related to the theory of high-order statistics (based on statistical expectations of the signals), by ways of statistical moments and cumulants. This section reviews the fundamentals of the HOCS theory and highlights the metrics that can be used for spectrum sensing.

4.1. Lag-Product. We must always keep in mind that the goal of the HOCS theory is to extract sine-waves components

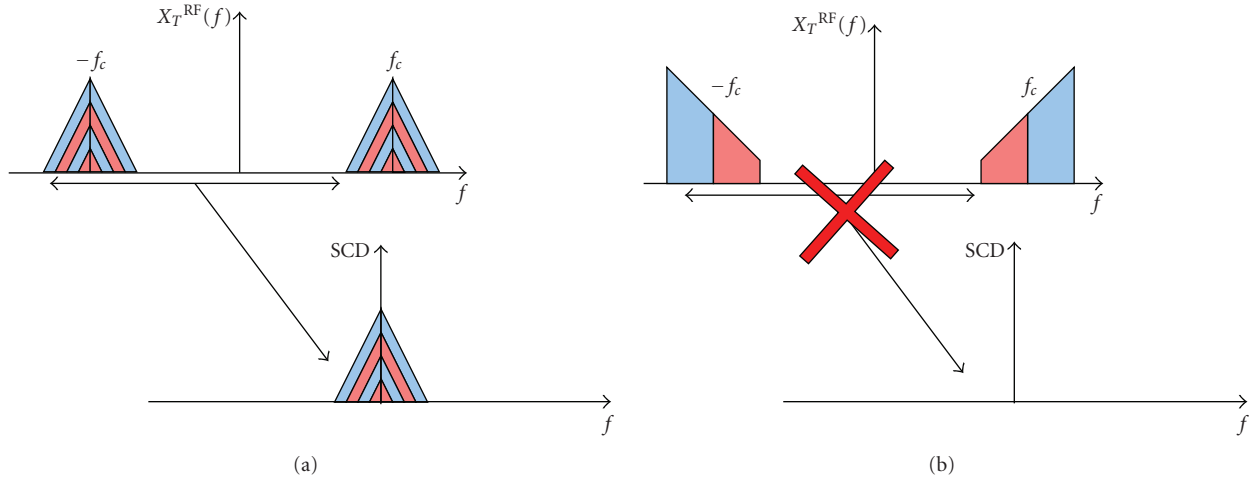

Figure 2: RF signal frequency spectrum (top) and SCD at twice the carrier frequency (bottom). The SCD is measured by the correlation between two frequency bins centered on $f - \alpha/2$ and $f + \alpha/2$ where α is the carrier frequency. The doubled-carrier frequency feature exists for RF PAM signals as the baseband frequency spectrum exhibits a correlation between negative and positive frequencies. In the absence of any filtering, this correlation produces a symmetric frequency spectrum (left part). The doubled-carrier frequency feature vanishes for RF QAM signals as the baseband frequency spectrum is uncorrelated (right part).

from a signal, in which they are hidden by random phenomena. To extract, or regenerate, these frequencies, a nonlinear operation must be called upon. The second-order theory uses the time-delay product $L(t,\tau) = x(t) \cdot x^*(t-\tau)$ which will be transformed in the autocorrelation after averaging. A natural and intuitive generalization of this operation to the nth-order is called the lag-product and can be expressed as [9]:

$$L(t,\underline{\tau})_n = x^{(*)}(t+\tau_1)x^{(*)}(t+\tau_2)\cdots x^{(*)}(t+\tau_n) \quad (9)$$

$$= \prod_{j=1}^{n} x^{(*)_j}\left(t+\tau_j\right), \quad (10)$$

where the vector $\underline{\tau}$ is composed of the individual delays τ_j $(j = 1,\ldots,n)$. The notation $x^{(*)}(t)$ indicates an optional conjugation of the signal $x(t)$.

4.2. Temporal Moment Function and Cyclic Temporal Moment Function. If the signal possesses a nth-order sine-wave of frequency α, then the averaging of the lag-product, multiplied by a complex exponential of frequency α, must be different from zero [9]:

$$R_x^{\alpha}(\underline{\tau})_n = \lim_{T\to\infty} \frac{1}{T} \int_{-T/2}^{T/2} L(t,\underline{\tau})_n e^{-j2\pi\alpha t} dt. \quad (11)$$

Obviously, $R_x^{\alpha}(\underline{\tau})_n$ is a generalization of the cyclic autocorrelation function described in (5). It is called the nth-order cyclic temporal moment function (CTMF). The sum of the CTMF (multiplied by the corresponding complex exponentials) over frequency α is called the temporal moment function (TMF) and is a generalization of the autocorrelation function described in (3):

$$R_x(t,\underline{\tau})_n = \sum_{\alpha} R_x^{\alpha}(\underline{\tau})_n e^{j2\pi\alpha t}. \quad (12)$$

Each term of the sum in (12) is called an impure nth-order sine-wave. This is so because the CTMF may contain products of lower-order sine-waves whose various orders sum to n. In order to extract the pure nth-order sine-wave from the lag-product, it is necessary to subtract the lower-order products. The pure nth-order sine-wave counter-part of the CTMF, denoted by $C_x^{\alpha}(\underline{\tau})_n$, is called the cyclic temporal cumulant function (CTCF). The pure nth-order sine wave counter-part of the TMF, denoted by $C_x(t,\underline{\tau})_n$, is called the temporal cumulant function (TCF).

4.3. Temporal Cumulant Function and Cyclic Temporal Cumulant Function. The CTMF and TMF have been computed by using the FOT probability framework. In order to compute the CTCF and TCF, it is interesting to make use of the equivalence between the FOT probability framework and the high-order statistics theory. More specifically, the paper [9] demonstrates that the TMF of a signal can be seen as the nth-order moment of the signal, and that the TCF of a signal can be seen as the nth-order cumulant of the signal (hence their names). By using the conventional relations between the moments and the cumulants found in the high-order statistics theory, the TCF takes therefore the form:

$$C_x(t,\underline{\tau})_n = \sum_{\{P\}} \left[(-1)^{p-1}(p-1)! \prod_{j=1}^{p} R_x\left(t,\underline{\tau}_j\right)_{n_j} \right], \quad (13)$$

where $\{P\}$ denotes the set of partitions of the index set $1,2,\ldots n$ (10), p is the number of elements in the partition P, and $R_x(t,\underline{\tau}_j)_{n_j}$ is the TMF of the jth-element of order n_j of the partition P.

The CTCFs are the Fourier coefficients of the TCF and can be expressed in terms of the CTMFs:

$$C_x^{\alpha}(\underline{\tau})_n = \sum_{\{P\}} \left[(-1)^{p-1}(p-1)! \sum_{\{\underline{\beta}\}} \prod_{j=1}^{p} R_x^{\beta_j}\left(\underline{\tau}_j\right)_{n_j} \right], \quad (14)$$

where $\{\underline{\beta}\}$ denotes the set of vectors of cycle frequencies for the partition P that sum to α ($\sum_{j=1}^{p} \beta_j = \alpha$), and $R_x^{\beta_j}(\underline{\tau}_j)_{n_j}$ is the CTMF of the jth-element of order n_j of the partition P at the cycle frequency β_j.

The CTCF is periodic in $\underline{\tau}$: $C_x^{\alpha}(\underline{\tau}+\underline{1}_n\ \phi)_n = C_x^{\alpha}(\underline{\tau})_n\ e^{j2\pi\phi\alpha}$ ($\underline{1}_n$ is the dimension-n vector composed of ones, meaning that ϕ is added to all elements of $\underline{\tau}$). Therefore, it is not absolutely integrable in $\underline{\tau}$. To circumvent this problem, one dimension is fixed (e.g., $\tau_n = 0$), and the CTCF becomes: $\overline{C}_x^{\alpha}(\underline{u})_n = C_x^{\alpha}([\underline{u}\ 0])_n$. This function is called reduced dimension-CTCF (RD-CTCF). It is the key metric of the ensuing algorithms for HOCS detectors. It should be noted that the equivalent exists for the CTMF and is called the RD-CTMF ($\overline{R}_x^{\alpha}(\underline{u})_n = R_x^{\alpha}([\underline{u}\ 0])_n$). However the RD-CTMF is generally not absolutely integrable.

4.4. Cyclic Polyspectrum. The need for integrability comes from the desire to compute the Fourier transform of the RD-CTCF, which gives the cyclic polyspectrum (CP). The CP is a generalization of the SCD plane for cyclostationnary signals. However it is not necessary to compute the CP of a signal for sensing applications since detection statistics can be directly derived from a single slice of the RD-CTCF. For this reason, and the computational complexity gain, we will put the spectral parameters aside and devote our attention to the RD-CTCF.

5. Fourth-Order Features of Linearly Modulated Signals

We have previously talked about the second-order cyclic features for communication signals, and we saw that the carrier frequency features tend to vanish from the SCD plane if the modulation is complex. We also asked ourselves if a fourth-order transformation of the signal may suppress the destructive interferences of quadrature components of a signal. We now have to gauge the potential of these fourth-order features. In this section, we compute the RD-CTCF of the baseband and RF linearly modulated signals and identify the interesting features that can be used for signal detection.

5.1. Baseband Signals. The TCF of the baseband signal (1) has been computed in paper [10]. The mathematical derivation results in:

$$C_s(t,\tau)_n = C_{I,n} \sum_{m=-\infty}^{\infty} \prod_{j=1}^{n} p\left(t + mT_s + \tau_j\right) \quad (15)$$

in which $C_{I,n}$ is the nth-order cumulant of the symbol sequence I_m:

$$C_{I,n} = \sum_{\{P_n\}} \left[(-1)^{p_n-1}\ (p_n-1)! \prod_{j=1}^{p_n} R_{I,n_j} \right], \quad (16)$$

where $\{P_n\}$ is the set of partitions of the set $\{1,\ldots,n\}$, p_n is the number of elements in the partition P_n, and n_j is the order of the jth-element in the partition P_n ($j = 1 \cdots p_n$). $R_{I,n}$ is the nth-order moment of the symbol sequence I_m:

$$R_{I,n} = \lim_{K\to\infty} \frac{1}{K} \sum_{k=-K/2}^{K/2-1} \left[\prod_{q=1}^{n} I_k^{(*)_q} \right]. \quad (17)$$

The expression of the moment $R_{I,n}$ can be understood this way: given a particular type of modulation, do the symbol variables I_k elevated to the power n (with optional conjugation specified by the operator $(*)_q$) gives a constant result? The answer to this question is helpful in assessing if a given signal may exhibit nth-order features and what kind of conjugation must be used in the lag-product (10). The appendix illustrates this result for the binary PAM and the quaternary QAM constellations (see also [10, 15]).

Computing the Fourier transform of the TCF and canceling τ_n reveals the RD-CTCF in the form of:

$$\overline{C}_s^{\alpha}(\underline{u})_n = \frac{C_{I,n}}{T_s} \int_{t=-\infty}^{\infty} p^{(*)}(t) \prod_{j=1}^{n-1} p^{(*)}\left(t+u_j\right) e^{-j2\pi\alpha t} dt, \quad (18)$$

where the cycle frequencies are integer multiples of the symbol rate ($\alpha = kF_s$ with k integer). The RD-CTCF of the baseband signal is nonzero only for harmonics of the symbol rate. The amplitude of the features tend to zero as the harmonic number k increases.

5.2. RF Signals. The RD-CTCF of the RF signal specified by (2) can be inferred from the RD-CTCF of the baseband signal $s(t)$ by noting that the RF signal is obtained by modulating two independent PAM signals in quadrature. We need to calculate the CTCFs of PAM, sine and cosine signals, and to combine them using the following rules:

(i) The cumulant of the sum is equal to the sum of the cumulants if the signals are independent. Therefore, if $y(t) = x(t) + w(t)$ where $x(t)$ and $w(t)$ are two independent random signals, we have:

$$C_y(t,\underline{\tau})_n = C_x(t,\underline{\tau})_n + C_w(t,\underline{\tau})_n \quad (19)$$

and, after Fourier transform, we obtain:

$$C_y^{\alpha}(\underline{\tau})_n = C_x^{\alpha}(\underline{\tau})_n + C_w^{\alpha}(\underline{\tau})_n. \quad (20)$$

(ii) The moment of the product is equal to the product of the moments if the signals are independent. Therefore, if $y(t) = x(t)\ w(t)$ where $x(t)$ and $w(t)$

are two independent random signals, we have:

$$R_y(t,\underline{\tau})_n = R_x(t,\underline{\tau})_n R_w(t,\underline{\tau})_n \tag{21}$$

and, after Fourier transform, we obtain:

$$R_y^{\alpha}(\underline{\tau})_n = \sum_{\gamma} R_x^{\alpha-\gamma}(\underline{\tau})_n R_w^{\gamma}(\underline{\tau})_n. \tag{22}$$

Equation (22) means that we have to multiply all CTMFs of $x(t)$ and $w(t)$ which sum to α. If one of the signals is nonrandom ($w(t)$ in our case), the CTMF of the random signal can be replaced by its CTCF:

$$C_y^{\alpha}(\underline{\tau})_n = \sum_{\gamma} C_x^{\alpha-\gamma}(\underline{\tau})_n \; R_w^{\gamma}(\underline{\tau})_n. \tag{23}$$

The CTCFs of the baseband PAM signals can be computed using (18). The only difference with a QAM signal resides in the cumulant of the symbol sequence $C_{I,n}$, which must be computed for PAM symbols through (16) and (17) (see the binary PAM case in the appendix).

The CTMF of the sine and cosine signals can easily be determined from the expression of their lag-products:

$$\begin{aligned} R_{\cos}^{\alpha}(t,\underline{\tau})_n &= \lim_{T\to\infty}\frac{1}{T}\int_{-T/2}^{T/2}\prod_{j=1}^{n}\cos\left(\omega_c t+\phi_j\right)e^{-i2\pi\alpha t}dt \\ R_{\sin}^{\alpha}(t,\underline{\tau})_n &= \lim_{T\to\infty}\frac{1}{T}\int_{-T/2}^{T/2}\prod_{j=1}^{n}\sin\left(\omega_c t+\phi_j\right)e^{-i2\pi\alpha t}dt, \end{aligned} \tag{24}$$

where $\phi_j = \omega_c\tau_j$. The lag-product can be decomposed into a sum of cosine signals at various frequencies using Simpson formulas:

$$\begin{aligned} L_{\cos}(t,\underline{\tau})_2 &= \frac{1}{2}\cos(2\omega_c t+\phi_1+\phi_2)+\frac{1}{2}\cos(\phi_1-\phi_2) \\ L_{\sin}(t,\underline{\tau})_2 &= -\frac{1}{2}\cos(2\omega_c t+\phi_1+\phi_2)+\frac{1}{2}\cos(\phi_1-\phi_2) \end{aligned} \tag{25}$$

for the second order, and:

$$\begin{aligned} L_{\cos}(t,\underline{\tau})_4 = {} & \frac{1}{8}\cos(4\omega_c t-\phi_1-\phi_2-\phi_3-\phi_4) \\ & +\frac{1}{8}\left(\cos(2\omega_c t+\phi_1+\phi_2+\phi_3-\phi_4)\right. \\ & \quad +\cos(2\omega_c t+\phi_1+\phi_2-\phi_3+\phi_4) \\ & \quad +\cos(2\omega_c t+\phi_1-\phi_2+\phi_3+\phi_4) \\ & \quad \left.+\cos(2\omega_c t-\phi_1+\phi_2+\phi_3+\phi_4)\right) \\ & +\frac{1}{8}\left(\cos(\phi_1-\phi_2+\phi_3-\phi_4)\right. \\ & \quad +\cos(\phi_1-\phi_2-\phi_3+\phi_4) \\ & \quad \left.+\cos(\phi_1+\phi_2-\phi_3-\phi_4)\right) \\ L_{\sin}(t,\underline{\tau})_4 = {} & \frac{1}{8}\cos(4\omega_c t-\phi_1-\phi_2-\phi_3-\phi_4) \\ & -\frac{1}{8}\left(\cos(2\omega_c t+\phi_1+\phi_2+\phi_3-\phi_4)\right. \\ & \quad +\cos(2\omega_c t+\phi_1+\phi_2-\phi_3+\phi_4) \\ & \quad +\cos(2\omega_c t+\phi_1-\phi_2+\phi_3+\phi_4) \\ & \quad \left.+\cos(2\omega_c t-\phi_1+\phi_2+\phi_3+\phi_4)\right) \\ & +\frac{1}{8}\left(\cos(\phi_1-\phi_2+\phi_3-\phi_4)\right. \\ & \quad +\cos(\phi_1-\phi_2-\phi_3+\phi_4) \\ & \quad \left.+\cos(\phi_1+\phi_2-\phi_3-\phi_4)\right) \end{aligned} \tag{26}$$

for the fourth order. It is clear that the CTMF of sine or cosine signals is made of Dirac's deltas at cycle frequencies $4f_c$, $2f_c$, and 0.

Since the real and imaginary parts of $s(t)$ are two statistically independent PAM signals, the CTCF of $s^{\mathrm{RF}}(t)$ is the sum of two CTCFs of modulated PAM signals in quadrature. The CTCFs of $\Re[s(t)]$ and $\Im[s(t)]$ are equal and denoted by $C_{\mathrm{PAM}}^{\alpha}(\underline{\tau})_n$ in our next results. We can finally write:

$$\overline{C}_{s^{\mathrm{RF}}}^{\alpha}(\underline{u})_n = \sum_{\gamma}\overline{C}_{\mathrm{PAM}}^{\alpha-\gamma}(\underline{u})_n\left(\overline{R}_{\cos}^{\gamma}(\underline{u})_n+\overline{R}_{\sin}^{\gamma}(\underline{u})_n\right). \tag{27}$$

For $n = 2$, we observe the destructive interference between the components of $\overline{R}_{\cos}^{\gamma}(\underline{u})_2$ and $\overline{R}_{\sin}^{\gamma}(\underline{u})_2$ at twice the carrier frequency, as was introduced in Section 3.

For $n = 4$, we also observe that the components of $\overline{R}_{\cos}^{\gamma}(\underline{u})_4$ and $\overline{R}_{\sin}^{\gamma}(\underline{u})_4$ at twice the carrier frequency cancel out, just as they do for the second order. There only remain the features at zero and four times the carrier frequency:

$$\begin{aligned} \overline{C}_s^0(\underline{u})_4 &\simeq \overline{C}_{\mathrm{PAM}}^0(\underline{u})_4\left(\overline{R}_{\cos}^0(\underline{u})_4+\overline{R}_{\sin}^0(\underline{u})_4\right) \\ &= 2\overline{C}_{\mathrm{PAM}}^0(\underline{u})_4\overline{R}_{\cos}^0(\underline{u})_4 \\ \overline{C}_s^{4f_c}(\underline{u})_4 &\simeq \overline{C}_{\mathrm{PAM}}^0(\underline{u})_4\left(\overline{R}_{\cos}^{4f_c}(\underline{u})_4+\overline{R}_{\sin}^{4f_c}(\underline{u})_4\right) \\ &= 2\overline{C}_{\mathrm{PAM}}^0(\underline{u})_4\overline{R}_{\cos}^{4f_c}(\underline{u})_4. \end{aligned} \tag{28}$$

Since $\overline{R}_{\cos}^0(\underline{u})_4$ is a sum of cosines that depend on $\underline{u}$ and $\overline{R}_{\cos}^{4f_c}(\underline{u})_4 = (1/16)e^{j\omega_c\sum(-)_i\phi_i}$ (the notation $(-)_i$ indicates an optional sign change according to the expressions (25)-(26)), the features $\overline{C}_s^{4f_c}(\underline{u})_4$ are six times smaller than the features $\overline{C}_s^0(\underline{u})_4$ (at least when $\underline{u}$ is null) and are therefore less suited for sensing scenarios.

5.3. Baseband and RF Fourth-Order Features. We have to choose between baseband or RF signals and decide on the cycle frequency that will be used by the detector. We have seen that baseband QAM signals have features at the cycle frequencies that are multiples of the symbol rate $(0, F_s, 2F_s\ldots)$, whereas RF signals have additional features

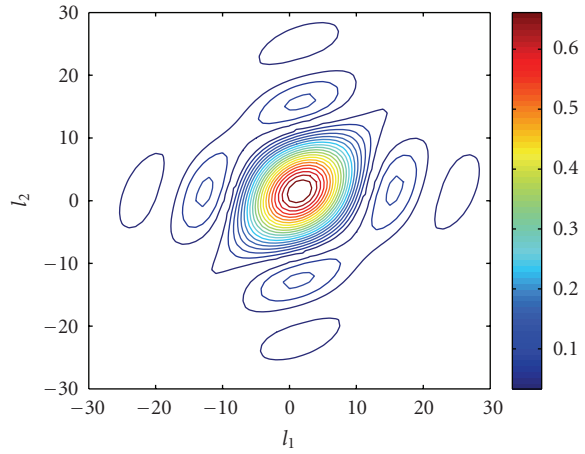

Figure 3: Fourth-order RD-CTCF of a 4-QAM baseband signal as a function of the lag parameters l_1 and l_2 for the cycle frequency 0. The values of l_0 and l_3 have been fixed to 0 and 3 respectively. The system parameters are: 1 MHz symbol frequency, 10 MHz sample frequency, normalized square-root Nyquist pulse shaping filter of 0.2 roll-off factor.

at cycle frequencies that depend on the carrier frequency ($4fc + 0$, $4fc + F_s$, $4fc + 2F_s \ldots$). It has been shown that these additional features are small and that the strongest feature for both baseband and RF signals is obtained when the cycle frequency α is equal to zero. Since noise signals do not have any fourth-order feature (the fourth-order cumulant of a Gaussian random variable is equal to zero), even when $\alpha = 0$. Note that $\alpha = 0$ is a degenerated cycle frequency, which is present even in stationary signals. However, since it gives the strongest 4th-order feature, it is the frequency that will be preferred for our sensing scenario, even if the denomination "cyclic-feature detector" becomes inappropriate in this case.

Simulations made with baseband or RF signals for $\alpha = 0$ have shown that the two detectors exhibit similar performances. From now on, we will focus on the fourth-order feature detection for baseband signals and let aside the fourth-order feature detection for RF signals, as it enables a significant reduction of the received signal sampling frequency. The feature obtained in this situation is illustrated in Figure 3.

6. Fourth-Order Feature Detectors

6.1. RD-CTCF Estimator. In order to estimate the RD-CTCF of the baseband QAM signal, we would have to use (14). Luckily, the signal is complex and the second order features disappear if we do not use any conjugation in the lag product (see the quaternary QAM example in the appendix). Therefore the RD-CTCF is equal to the RD-CTMF:

$$\overline{C}_s^0(\underline{u})_4 = \overline{R}_s^0(\underline{u})_4 = \lim_{T\to\infty} \frac{1}{T} \int_{-T/2}^{T/2} L_s(t, \underline{u})_4 dt \qquad (29)$$

In practice, the RD-CTCF is estimated based on a size-N finite observation window of the received sequence $s[n]$ obtained after sampling the received signal.

$$\widehat{\overline{C}}_s[\underline{l}]_4 = \frac{1}{N} \sum_{n=-N/2}^{N/2-1} L_s[n, \underline{l}]_4 \qquad (30)$$

with $N > 2\max|l_j|$ and l_j are the elements of the discrete lag-vector $\underline{l}$ of size $n-1$.

6.2. Noise Mean and Variance. When there is only noise in the system, the mean of the RD-CTCF is equal to 0 since the fourth-order cumulant of a Gaussian random variable is null. On the other hand, the variance of the RD-CTCF is a function of the lag-vector given by:

$$\sigma^2_{\text{RD-CTCF}} = \begin{cases} \frac{1}{N}\sigma_n^8 & \text{if all lag values are different} \\ \frac{2}{N}\sigma_n^8 & \text{if two lag values are equal} \\ \frac{6}{N}\sigma_n^8 & \text{if three lag values are equal} \\ \frac{24}{N}\sigma_n^8 & \text{if all lag values are equal} \end{cases} \qquad (31)$$

in which σ_n^2 is the variance of AWGN noise samples at the input of the RD-CTCF estimator. Simulations illustrated in Figure 4 confirm the result (31). Every discrete lag-vector $\underline{l}$ for which two or more values l_i, l_j are identical should be avoided, since it increases the noise variance. However, to afford the luxury of choosing lag values that are different from zero, we would have to increase the sampling rate at the receiver, which in turn would increase the noise power. Simulations have shown that it is better to use the lowest sampling rate that still satisfies Shannon's theorem, and set all lag values equal to zero. The RD-CTCF variance also quite naturally decreases as the observation window N is increased.

6.3. Detector. The detector has to decide between two hypotheses: hypothesis H_0 implying that no signal is present, hypothesis H_1 implying that the linearly modulated signal is present. The absolute value of the feature (here the RD-CTCF) is compared to a threshold γ to make a decision:

$$\left|\widehat{\overline{C}}_s^0(\underline{l})_4\right| \underset{H_0}{\overset{H_1}{\gtrless}} \gamma. \qquad (32)$$

The threshold is usually fixed to meet a target probability of false alarm (decide H_1 if H_0). In order to compute the threshold level as a function of the probability of false alarm, we must know the distribution of the RD-CTCF. We already know its mean and variance values and using the central-limit theorem, we assume that the output distribution is Gaussian (see also [16]). As a consequence, the absolute value of the RD-CTCF takes the form of a Rayleigh distribution and the threshold level can be found using:

$$\gamma = \sqrt{-\sigma^2_{\text{RD-CTCF}} \ln P_{fa}}, \qquad (33)$$

where P_{fa} is the probability of false alarm.

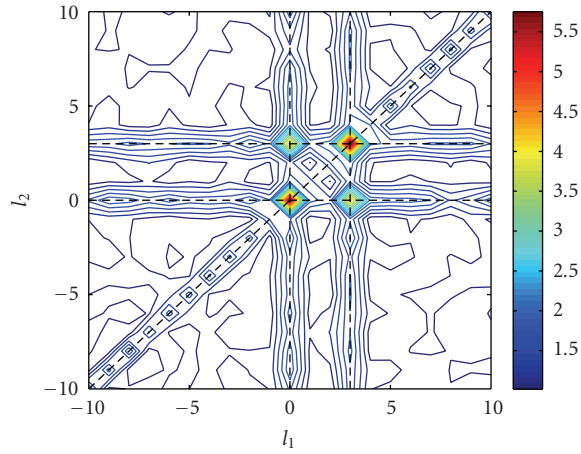

FIGURE 4: Noise variance at the output of the RD-CTCF estimator as a function of the lag parameters l_1 and l_2 for the cycle frequency 0. The values of l_0 and l_3 have been fixed to 0 and 3, respectively. The system parameters are: 1 MHz symbol frequency, 10 MHz sample frequency, $\sigma_n^2 = 10$. The number of noise realizations is 1000.

7. Detector Comparison

We will now briefly review the principles of all detectors previously mentioned in this paper, and compare their performance and computational complexity. We assume that second-order and fourth-order detectors work only at a single location of the feature they exploit (the second-order detector works at most favorable frequency, the fourth-order detector works at the most favorable value of the discrete lag-vector l). Monte-Carlo simulations were used, each of which used 5000 iterations.

7.1. Energy Detector. This is the most widely used detector in wireless communication systems. It averages the square modulus of the received sequence over time:

$$\rho_{\mathrm{ED}} = \frac{1}{N}\sum_{n=-N/2}^{N/2-1} |s[n]|^2. \tag{34}$$

Its advantages are its simplicity and its ability to perform blind detection (since it does not require any information about the signal it is trying to detect). Unfortunately, it has been demonstrated that it cannot be used in low-SNR environments due to its sensitivity to noise uncertainty [6].

7.2. Second-Order Detector. This detector computes an estimation of the SCD by averaging, over time and frequency domains, the cyclic periodogram of the signal spectrum $S_k(f)$ computed for a finite time window at time k:

$$\rho_{\mathrm{CF2}} = \frac{1}{K}\frac{1}{F}\sum_{k=-K/2}^{K/2-1}\sum_{u=-F/2}^{F/2-1} S_k\left(f+u-\frac{\alpha}{2}\right) S_k^*\left(f+u+\frac{\alpha}{2}\right), \tag{35}$$

where K is the number of time windows and F is the number of frequency bins. It is a much more complex and less efficient detector, which requires some characteristics of the signal in order to work (e.g., the symbol rate must be known in advance). Its advantage resides in the absence of features (at least asymptotically) when the input signal is a white noise, which results in the output mean of the detector always being equal to zero in presence of noise, therefore shielding the detector from noise uncertainty effects. Its computational complexity evolves as $N \cdot \log_2(1024) = N.10$ if the FFTs used to evaluate the cyclic periodogram [6] have a length of 1024 samples, and the total number of samples is equal to N.

7.3. Fourth-Order Detector. This detector averages the lag-product of the received sequence over time:

$$\rho_{CF4} = \frac{1}{N}\sum_{n=-N/2}^{N/2-1} s[n]s[n+l_1]s[n+l_2]s[n+l_3]. \tag{36}$$

This detector is simpler to implement than the previous one (no Fourier transform of the signal is required since we work in the time domain), which results in a computational complexity evolving as N, the total number of samples. It benefits from the same immunity to noise uncertainty, and is therefore suited for operations at low SNR.

7.4. Performance Comparison. We may now take a look at the performance of the different detectors. Figure 5 illustrates the probability of missed detection (decide H_0 if H_1) curves as a function of the SNR for the three detectors under consideration. The threshold has been set in the three cases to achieve a target probability of false alarm equal to 10^{-1}. These curves have been obtained without adding any noise uncertainty to the signal. In such conditions, the energy detector is the optimal detector for blind detection, and can be considered as a reference. It appears that the second-order detector and the fourth-order detector, have similar performances when the SNR is around zero dB: for the same complexity, (that leads to an observation time ten times longer for the fourth-order detector), both detectors exhibit the same probability of missed detection (roughly 1 percent) at an SNR of −0.8 dB. However, when we consider an SNR of −4 dB, the fourth-order detector requires much more samples, which makes it more complex than the second-order. Besides, the detection-time constraints that are part of the cognitive radios reglementation would not be met if the observation time is too long.

If we add some amount of noise uncertainty, the energy detector cannot perform reliable detections and must be discarded, whereas the cyclic feature detectors remain unaffected. In order to verify this assumption, we computed the receiver operating characteristics (ROC) curves of the fourth-order detector for two situations, one without any noise uncertainty, and one with 0 dB of noise uncertainty. The results are illustrated in Figure 6. We observe that the energy detector, which had the best ROC curve in the first case is a lot more affected by the noise uncertainty than the fourth-order detector. ROC curves for the second-order detector can be found in [7], and show the same immunity to noise uncertainty than the fourth-order.

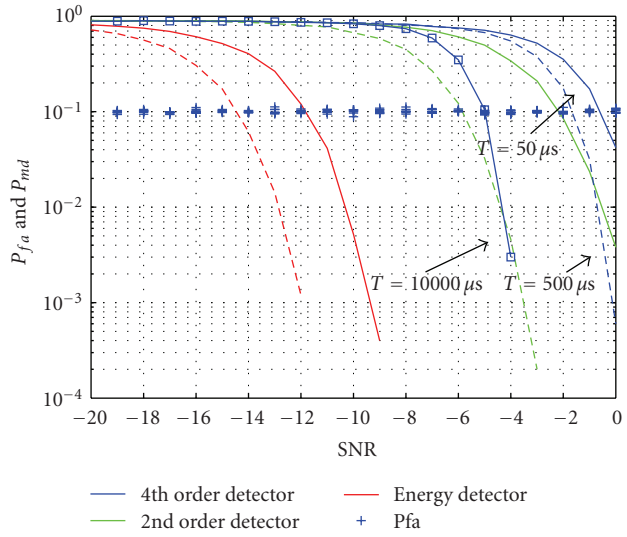

FIGURE 5: Energy, second-order and fourth-order detector probability of missed detection (the solid lines) for a fixed probability of false alarm (the points at 10^{-1}). The system parameters are: baseband QPSK signal with 20 MHz symbol frequency, 40 MHz sample frequency, square-root Nyquist pulse shaping filter of 0.2 roll-off factor. No noise uncertainty added. The second-order detector is set to detect the symbol-rate feature (cf = 20 MHz), and the fourth-order detector works with the feature at four-times the carrier frequency, which is equal to zero in the present situation (cf = 0 MHz).Two observation times are considered for the three detectors: 50 and 500 μs. An observation time of 10 ms has been added for the fourth-order detector

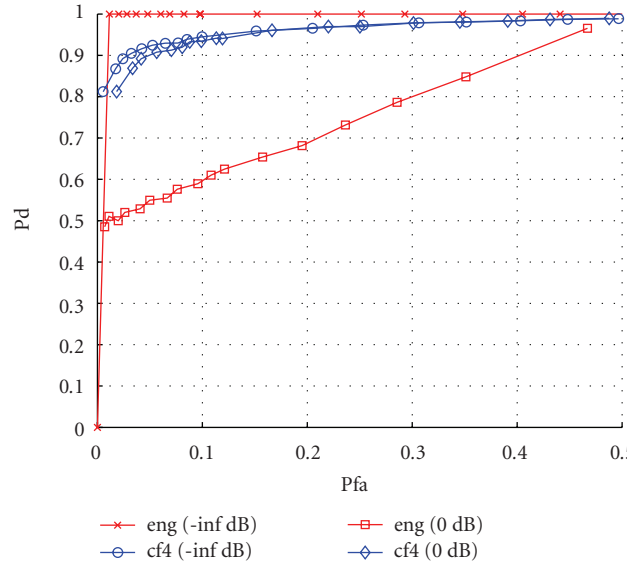

FIGURE 6: Energy (eng) and fourth-order detector (cf4) ROC curves for two values of the noise uncertainty (no uncertainty, 0 dB uncertainty). The system parameters are: 1 MHz symbol frequency, 4 MHz sample frequency, square-root Nyquist pulse shaping filter of 0.2 roll-off factor, SNR = −2 dB.

8. Conclusion

This paper has started from the need for robust detectors able to work in low SNR environments. A brief review of the second-order cyclostationarity and second-order cyclic feature detectors has exposed the advantages and drawbacks of such detectors, and explained the intuition that lead to the study of higher-order cyclostationarity (HOCS). The main guideline is to identify features of sufficient strength and to design a detector able to extract it from the signal. The most relevant aspects of HOCS theory have then been analyzed and we have derived a new fourth-order detector that can be used for the detection of linearly modulated signals. Simulation results have shown that fourth-order cyclic feature detectors may be used as a substitute for second-order detectors at SNR around zero dB, which could be needed if the received signals do not exhibit second-order cyclostationarity.

Appendices

A. Cumulants of the Binary PAM

This section computes the second- and fourth-order cumulants of a binary PAM sequence. The symbols take the values $I_m = \{\pm 1\}$.

A.1. Second-Order Cumulant. There are 2 possible partitions of the set $\{1,2\}$: $\{1,2\}$ and $\{1\}\{2\}$. Since the binary PAM constellation is symmetric, only the first partition has a chance to give a product of moments different from 0. We will limit our investigations to the first partition.

The partition $\{1,2\}$ gives $R_{I,2} = 1$ for its single element, so that $C_{I,2} = 1$.

A.2. Fourth-Order Cumulant. There are 14 possible partitions of the set $\{1,2,3,4\}$, but only the ones that group I_k by two or four have a chance to give a product of moments different from 0, which reduces the number of interesting partitions to four: $\{1,2,3,4\}$; $\{1,2\}\{3,4\}$; $\{1,3\}\{2,4\}$ and $\{1,4\}\{2,3\}$.

The first partition $\{1,2,3,4\}$ gives $R_{I,4} = 1$ for its single element, and the three last partitions $\{1,2\}\{3,4\}$; $\{1,3\}\{2,4\}$ and $\{1,4\}\{2,3\}$ give $R_{I,2} = 1$ for their two elements, so that $C_{I,4} = -2$.

B. Cumulants of the Quaternary QAM

This section computes the second- and fourth-order cumulants of a 4-QAM sequence. The symbols take the values $I_m = \{\pm 1/\sqrt{2} \pm j/\sqrt{2}\}$.

B.1. Second-Order Cumulants. There are 2 possible partitions of the set $\{1,2\}$: $\{1,2\}$ and $\{1\}\{2\}$. Since the 4-QAM constellation is symmetric, only the first partition has a chance to give a product of moments different from 0. We limit therefore our investigations to the first partition.

Different results are obtained according to the number of conjugations in the lag-product (10):

(i) When no conjugation or two conjugations are used in the lag-product, the partition $\{1,2\}$ gives $R_{I,2} = 0$ for its single element, so that $C_{I,2} = 0$.

(ii) When one conjugation is used in the lag-product, the partition $\{1,2\}$ gives $R_{I,2} = 1$ for its single element, so that $C_{\mathrm{I},2} = 1$.

B.2. Fourth-Order Cumulant. There are 14 possible partitions of the set $\{1,2,3,4\}$, but only the ones that group I_k by two or four have a chance to give a product of moments different from 0, which reduces the number of interesting partitions to four: $\{1,2,3,4\}$; $\{1,2\}\{3,4\}$; $\{1,3\}\{2,4\}$ and $\{1,4\}\{2,3\}$.

Different results are obtained according to the number of conjugations in the lag-product (10):

(i) When no conjugation or four conjugations are used in the lag-product, the first partition $\{1,2,3,4\}$ gives $R_{I,4} = -1$ for its single element, and the three last partitions $\{1,2\}\{3,4\}$; $\{1,3\}\{2,4\}$ and $\{1,4\}\{2,3\}$ give $R_{I,2} = 0$ for their two elements, so that $C_{I,4} = -1$.

(ii) When two conjugations are used in the lag-product, arbitrary placed for this example on the second and fourth element of the lag-product, the partition $\{1,2,3,4\}$ gives $R_{I,4} = 1$ for its single element, the two partitions $\{1,2\}\{3,4\}$ and $\{1,4\}\{2,3\}$ give $R_{I,2} = 1$ for their two elements, and the partition $\{1,3\}\{2,4\}$ gives $R_{I,2} = 0$ for its two elements, so that $C_{I,4} = -1$.

(iii) When one or three conjugations are used in the lag-product, the partition $\{1,2,3,4\}$ gives $R_{I,4} = 0$ for its single element, and the three last partitions $\{1,2\}\{3,4\}$; $\{1,3\}\{2,4\}$ and $\{1,4\}\{2,3\}$ give $R_{I,2} = 0$ for at least one of their two elements, so that $C_{I,4} = 0$.

References

[1] F. C. Commission, "FCC-03-322: Facilitating Opportunities for Flexible, Efficient, and Reliable Spectrum Use Employing Cognitive Radio Technologies," December 2003.

[2] I. F. Akyildiz, W.-Y. Lee, M. C. Vuran, and S. Mohanty, "NeXt generation/dynamic spectrum access/cognitive radio wireless networks: a survey," *Computer Networks*, vol. 50, no. 13, pp. 2127–2159, 2006.

[3] A. Sahai and D. Cabric, "Spectrum sensing: fundamental limits and practical challenges," in *Proceedings of IEEE International Symposium on New Frontiers in Dynamic Spectrum Access Networks (DySPAN '05)*, Baltimore, Md, USA, November 2005.

[4] H. Urkowitz, "Energy detection of unknown deterministic signals," *Proceedings of the IEEE*, vol. 55, no. 4, pp. 523–531, 1967.

[5] R. Tandra, *Fundamental limits on detection in low SNR*, M.S. thesis, Berkeley, Calif, USA, 2005.

[6] W. A. Gardner, "Signal interception: a unifying theoretical framework for feature detection," *IEEE Transactions on Communications*, vol. 36, no. 8, pp. 897–906, 1988.

[7] W. A. Gardner and C. M. Spooner, "Signal interception: performance advantages of cyclic-feature detectors," *IEEE Transactions on Communications*, vol. 40, no. 1, pp. 149–159, 1992.

[8] W. A. Gardner, *Statistical Spectral Analysis: A Nonprobabilistic Theory*, Prentice-Hall, Englewood Cliffs, NJ, USA, 1987.

[9] W. A. Gardner and C. M. Spooner, "Cumulant theory of cyclostationary time-series, part I: foundation," *IEEE Transactions on Signal Processing*, vol. 42, no. 12, pp. 3387–3408, 1994.

[10] C. M. Spooner and W. A. Gardner, "Cumulant theory of cyclostationary time series, part II: development and applications," *IEEE Transactions on Signal Processing*, vol. 42, no. 12, pp. 3409–3429, 1994.

[11] K. Kim, I. A. Akbar, K. K. Bae, J.-S. Um, C. M. Spooner, and J. H. Reed, "Cyclostationary approaches to signal detection and classification in cognitive radio," in *Proceedings of the 2nd IEEE International Symposium on New Frontiers in Dynamic Spectrum Access Networks (DySPAN '07)*, pp. 212–215, Dublin, Ireland, April 2007.

[12] P. D. Sutton, K. E. Nolan, and L. E. Doyle, "Cyclostationary signatures in practical cognitive radio applications," *IEEE Journal on Selected Areas in Communications*, vol. 26, no. 1, pp. 13–24, 2008.

[13] A. Tkachenko, D. Cabric, and R. W. Brodersen, "Cyclostationary feature detector experiments using reconfigurable BEE2," in *Proceedings of the 2nd IEEE International Symposium on New Frontiers in Dynamic Spectrum Access Networks (DySPAN '07)*, pp. 216–219, Dublin, Ireland, April 2007.

[14] V. Turunen, M. Kosunen, A. Huttunen et al., "Implementation of cyclostationary feature detector for cognitive radios," in *Proceedings of the 4th International Conference on Cognitive Radio Oriented Wireless Networks and Communications (CROWNCOM '09)*, Hannover, Germany, June 2009.

[15] O. A. Dobre, Y. Bar-Ness, and W. Su, "Higher-order cyclic cumulants for high order modulation classification," in *Proceedings of IEEE Military Communications Conference (MILCOM '03)*, pp. 112–117, October 2003.

[16] A. V. Dandawate and G. B. Giannakis, "Statistical tests for presence of cyclostationarity," *IEEE Transactions on Signal Processing*, vol. 42, no. 9, pp. 2355–2369, 1994.

Preliminary call for papers

The 2011 European Signal Processing Conference (EUSIPCO-2011) is the nineteenth in a series of conferences promoted by the European Association for Signal Processing (EURASIP, www.eurasip.org). This year edition will take place in Barcelona, capital city of Catalonia (Spain), and will be jointly organized by the Centre Tecnològic de Telecomunicacions de Catalunya (CTTC) and the Universitat Politècnica de Catalunya (UPC).

EUSIPCO-2011 will focus on key aspects of signal processing theory and applications as listed below. Acceptance of submissions will be based on quality, relevance and originality. Accepted papers will be published in the EUSIPCO proceedings and presented during the conference. Paper submissions, proposals for tutorials and proposals for special sessions are invited in, but not limited to, the following areas of interest.

Areas of Interest

- Audio and electro-acoustics.
- Design, implementation, and applications of signal processing systems.
- Multimedia signal processing and coding.
- Image and multidimensional signal processing.
- Signal detection and estimation.
- Sensor array and multi-channel signal processing.
- Sensor fusion in networked systems.
- Signal processing for communications.
- Medical imaging and image analysis.
- Non-stationary, non-linear and non-Gaussian signal processing.

Submissions

Procedures to submit a paper and proposals for special sessions and tutorials will be detailed at www.eusipco2011.org. Submitted papers must be camera-ready, no more than 5 pages long, and conforming to the standard specified on the EUSIPCO 2011 web site. First authors who are registered students can participate in the best student paper competition.

Important Deadlines:

Proposals for special sessions	15 Dec 2010
Proposals for tutorials	18 Feb 2011
Electronic submission of full papers	**21 Feb 2011**
Notification of acceptance	23 May 2011
Submission of camera-ready papers	6 Jun 2011

Webpage: www.eusipco2011.org

Organizing Committee

Honorary Chair
Miguel A. Lagunas (CTTC)

General Chair
Ana I. Pérez-Neira (UPC)

General Vice-Chair
Carles Antón-Haro (CTTC)

Technical Program Chair
Xavier Mestre (CTTC)

Technical Program Co-Chairs
Javier Hernando (UPC)
Montserrat Pardàs (UPC)

Plenary Talks
Ferran Marqués (UPC)
Yonina Eldar (Technion)

Special Sessions
Ignacio Santamaría (Unversidad de Cantabria)
Mats Bengtsson (KTH)

Finances
Montserrat Nájar (UPC)

Tutorials
Daniel P. Palomar (Hong Kong UST)
Beatrice Pesquet-Popescu (ENST)

Publicity
Stephan Pfletschinger (CTTC)
Mònica Navarro (CTTC)

Publications
Antonio Pascual (UPC)
Carles Fernández (CTTC)

Industrial Liaison & Exhibits
Angeliki Alexiou (University of Piraeus)
Albert Sitjà (CTTC)

International Liaison
Ju Liu (Shandong University-China)
Jinhong Yuan (UNSW-Australia)
Tamas Sziranyi (SZTAKI -Hungary)
Rich Stern (CMU-USA)
Ricardo L. de Queiroz (UNB-Brazil)